Patient-specific 3D Ultrasound Simulation Based on Convolutional Ray-tracing and Appearance Optimization

Mehrdad Salehi[1,3], Seyed-Ahmad Ahmadi[2], Raphael Prevost[1], Nassir Navab[3,4], and Wolfgang Wein[1]

[1] ImFusion GmbH, München, Germany
[2] Department of Neurology, Klinikum der Universität München, LMU, Germany
mehrdad.salehi@tum.de
[3] Computer Aided Medical Procedures, Technische Universität München, Germany
[4] Computer Aided Medical Procedures, Johns Hopkins University, Baltimore, USA

Abstract. The simulation of medical ultrasound from patient-specific data may improve the planning and execution of interventions e.g. in the field of neurosurgery. However, both the long computation times and the limited realism due to lack of acoustic information from tomographic scans prevent a wide adoption of such a simulation. In this work, we address these problems by proposing a novel efficient ultrasound simulation method based on convolutional ray-tracing which directly takes volumetric image data as input. We show how the required acoustic simulation parameters can be derived from a segmented MRI scan of the patient. We also propose an automatic optimization of ultrasonic simulation parameters and tissue-specific acoustic properties from matching ultrasound and MRI scan data. Both qualitative and quantitative evaluation on a database of 14 neurosurgical patients demonstrate the potential of our approach for clinical use.

1 Introduction

A realistic simulation of medical ultrasound is an important tool, e.g. for transducer design, training of physicians or multi-modal image-registration through simulation. A further attractive application is pre-operative planning, in which a patient-specific ultrasound simulation of the operational situs could help the surgeon to anticipate tissue appearance or optimal transducer positioning. However, a wide adoption in this context has been prevented by two problems. First, computation times of realistic ultrasound simulation methods still prevent interactive frame rates. Second, deriving the required acoustic parameters of tissue from a CT or MRI scan of the same patient is difficult due to different physical imaging principles and limited resolution of the source modalities. In this work, we are addressing both problems by proposing an interactive and realistic simulation based on convolution and ray-tracing with simulation parameters that can be optimized to match the appearance of real ultrasound images.

N. Navab et al. (Eds.): MICCAI 2015, Part II, LNCS 9350, pp. 510–518, 2015.
DOI: 10.1007/978-3-319-24571-3_61

Ultrasound simulation approaches can be roughly categorized into wave-based, ray-based and convolution-based methods. Wave-based methods offer the highest realism and physical accuracy due to actual simulation of wave-front propagation in tissue. However, they are computationally expensive, requiring up to one hour for rendering of a single frame even on modern graphic card hardware [9]. Another approach is to simulate the spatial impulse response of the ultrasound system and convolve it with an artificial map of micro-scatters. A well-known software to employ this model is Field II, which takes up to one minute for simulation of a 2D image [8] and often serves as gold standard in validation of other methods. Another convolution-based approach was introduced by Bamber [1] and expanded by Meunier [11], in which the image is created by convolution of the imaging system's point-spread-function (PSF) with a map of points representing the position and reflectivity of scatterers. A comparison study in [5] shows that recently proposed convolution-based method, COLE [4], can provide similar image quality and statistics compared to Field II, while offering real-time simulation speeds. A problem in these methods, however, is the inability to mimic specific types of US imaging artifacts such as refractions, mirroring, range distortion, shadowing, and enhancement.

Ray-based simulation techniques focus on generating real-time images using ray optics. They cover acoustic brightness of tissue regions, reflections at tissue boundaries and shadowing artefacts, but they are lacking speckle noise or reflection- and refraction-induced artefacts.

In [2], a computer graphics ray-tracing scheme is adapted for fast convolution-based ultrasound simulation. The ray-tracing depends on exact surface models of brain regions, requiring extensive pre-processing of the data and post-processing to overcome simplifications of the ray-based approach. We adopt and extend this method to work directly on volume data, which can be derived from a patient's MRI or CT in a number of simple image processing steps. Moreover, our method interleaves convolution and ray-tracing, such that scattering properties of the tissue are propagated throughout the entire ultrasound beam formation process. Additionally, we demonstrate for the first time a method to directly optimize ultrasound simulation parameters and acoustic properties of the underlying tissue maps through image-based matching of patient-specific ultrasound and MRI data. An overview of the proposed system is shown in Fig. 1.

2 Methods

2.1 Patient-Specific Acoustic Data from MRI

Six acoustic parameters are defined for each medium. Speed of sound c, acoustic impedance Z, and attenuation coefficient α are used in the ray-tracing engine to compute the intensity and relative time of the rays at each point. Three other parameters, μ_0, μ_1, and σ_0 drive a generative model for the distribution and intensity of scatterer points in each medium (detailed description in [2]). The ray-tracing part is performed on a label volume containing the tissue indices corresponding to the parameters table. The pre-processing part thus consists of segmenting and labeling the source modality, in our case MRI data.

A well-established approach for multi-class segmentation of MRI is to cluster image intensities using a Gaussian Mixture model and optimizing the fitting using the Expectation-Maximization (EM) algorithm [14]. Instead of enforcing spatial regularization during EM, we pre-process the MRI with a guided filter [6] which acts as a very fast anisotropic diffusion step. The resulting label maps are sufficiently smooth and accurate to be used as input to our simulation algorithm. No further processing or meshing of the segmentation is required.

2.2 Ultrasound Simulation

A ray-tracing engine is at the core of this method and builds the data for each radio frequency (RF) scanline separately. The recorded echo for each scanline i at the distance l from the transducer is defined as a sum of two main terms:

$$E_i(l) = R_i(l) + B_i(l) \tag{1}$$

where $R_i(l)$ is the reflected energy from the tissue boundaries and $B_i(l)$ is the backscattered energy from the scattering points throughout the scan line.

Reflection and Attenuation: We use a model similar to [13] to approximate both specular and diffuse reflections. Let $H(l)$ be the PSF of the imaging system, and $G(x, y, z)$ be an indicator function that returns 1 for points on the surface boundaries and 0 otherwise. Then, the reflected energy can be written as:

$$R_i(l) = \left| I_i(l) * \cos\theta_i{}^n * \left(\frac{Z_1 - Z_2}{Z_1 + Z_2}\right)^2 \right| * H(l) \otimes G(x, y, z) \tag{2}$$

The term $\cos\theta_i$ comes from Lambert's cosine law and θ_i is the angle of incidence. The exponent n is a simple modification to describe the heterogeneity on the surface and $I_i(l)$ is the remaining ultrasound wave amplitude. Z_1 and Z_2 are the acoustic impedances of two adjacent tissues. The sound energy gets attenuated during tissue traversal, which causes artefacts like shadowing and enhancement. The remaining energy of the sound beam $I_i(l)$ is modeled using the Beer-Lambert Law as $I_i(l) = I_0\ e^{-\alpha l f}$, where I_0 is the initial energy, f is the sound frequency, and α is the attenuation coefficient of the medium.

Backscattering Term: The other term in the returned echo, the back-scattered energy $B_i(l)$, is the product of the remaining wave amplitude and the convolution of the PSF $H(l)$ with random scatterers:

$$B_i(l) = I_i(l) * H(l) \otimes T(x, y, z). \tag{3}$$

Similar to [2], we create the scatterers from a generative model. It is based on two random textures which are combined using the tissue-specific parameters μ_0, μ_1, and σ_0. For each tissue, the model generates scatterers of various spatial and acoustic density. We refer the reader to [2] for details. The spatial PSF $H(x, y, z)$ (or $H(l)$ along the ray) is modeled with a cosine function modulated by a 3D

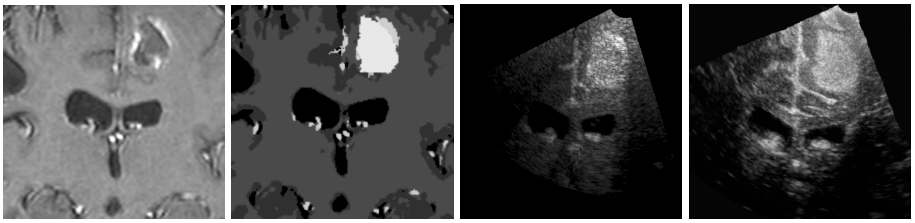

(a) MRI Volume (b) Segmented Data (c) Simulation (d) Real US Image

Fig. 1. Simulation/optimization pipeline; (a) Input modality, (b) Label-map after segmentation, (c) Simulation result before parameter optimization, (d) real US image, which is used for optimization of simulation parameters.

Gaussian envelope, which is sufficient to approximate the far-field [11]. The convolution kernel can be separated [1] into three 1D components, i.e. $H(x, y, z) = H_x(x) \times H_y(y) \times H_z(z)$, with an axial pulse $H_x(x) = \exp(-0.5x^2/\sigma_x^2)\cos(2\pi f x)$, and lateral and elevational beam profiles $H_y(y) = \exp(-0.5y^2/\sigma_y^2)$ and $H_z(z) = \exp(-0.5z^2/\sigma_z^2)$. The beam profile can thus be spatially varying, which allows for simulation of a sharper, user-defined focus zone and blurrier out-of-focus regions by dispersal of the beam profile. The convolution between the PSF and the scatterers texture is calculated during the entire ray-tracing for each pixel on the RF scan-lines.

Ray-Tracing: A binary tree structure keeps the data for the ray-tracing engine, which is based on optical principles. Each crossing of a ray with a tissue interface generates a reflected and a refracted ray, which are further traced into the medium. The remaining intensity (according to Fresnel equation), direction (according to Snell's law) and the relative time to transducer are passed to the child rays. The final result for each RF scan-line is the sum of all child rays covering that scan-line. Each ray terminates if (i) it leaves the imaging frame, (ii) its remaining intensity decreases lower than a user-defined threshold or (iii) its relative time to transducer exceeds the image penetration depth and thus the maximum allowed run-time. The whole simulation pipeline and post-processing steps are parallelized on GPU using OpenCL and OpenGL libraries, which makes it independent of proprietary ray-tracing engines as in [2].

Post-processing: Post-processing is performed using a simple RF to B-mode conversion scheme. We first add (Gaussian) amplifier noise to the signal and proceed with time gain compensation (TGC), envelope detection and dynamic range limiting of the signal [7]. The RF data is log-compressed and 8-bit quantized. Finally, the fan geometry and ultrasound image are calculated through scan conversion.

2.3 Automatic Optimization

We use registered MRI and 3D freehand ultrasound data from all 14 patients of the BITE neurosurgical database [10]. The following cost function is used in

a non-linear optimization of the simulation parameters with respect to the real ultrasound images as reference.

$$L(A, B) = \rho(A, B) + \lambda * \mathrm{SAD}(A, B) \tag{4}$$

$$\rho(A, B) = \frac{1}{N} \sum_{i}^{N} \sqrt{1 - \sum_{j}^{M} \sqrt{P_{ij} Q_{ij}}} \tag{5}$$

$\rho(A, B)$ is our proposed local Bhattacharyya distance between images A and B; P_i and Q_i are normalized distributions of patch number i of the images, M is the number of bins, and N is the number of patches. This is a modification of Bhattacharyya-based metric distribution distance proposed by Comaniciu *et al.* [3]. It caters to the fact that simulated speckle positions can not match with the real ultrasound, but their intensity distributions shall be similar. The localized version is required to prevent arbitrary configurations of tissue parameters which may nevertheless align the overall image histograms. We compute the average Bhattacharyya distance within local square image regions of width 5 mm. Through λ, it is weighted to the sum of absolute differences (SAD) of the image intensities. This assures the overall matching of large-scale structures, brightness and contrast. This measure, therefore, allows us to optimize (i) global post-processing parameters, which are typically unknown and different in every ultrasound acquisition and (ii) the acoustic parameters of each modeled tissue.

3 Evaluation

3.1 Acoustic Model

We demonstrate various US phenomena and artifacts of our simulation on a synthetic phantom. Obvious ones include shadowing or enhancement after high- or low-attenuation areas. Compared to purely ray-based or convolutional approaches, our hybrid algorithm can also simulate more subtle effects such as mirroring, reverberation or refraction at acoustic impedance interfaces, as well as geometric range distortions due to variations of speed of sound (Fig. 2).

3.2 Qualitative Results on Patient Data

We also illustrate the fidelity of our simulation using real-life, co-registered MRI and 3D US data from the BITE database. In Fig. 3, simulation results before and after optimization are shown alongside the real US image and MRI plane. Images are simulated using a pulse frequency of 5 MHz.

Direct comparison of this method to convolution-based approaches is challenging due to different scatterer map models. However, in future works our proposed similarity measure can be used for comparing different simulation approaches to real US data.

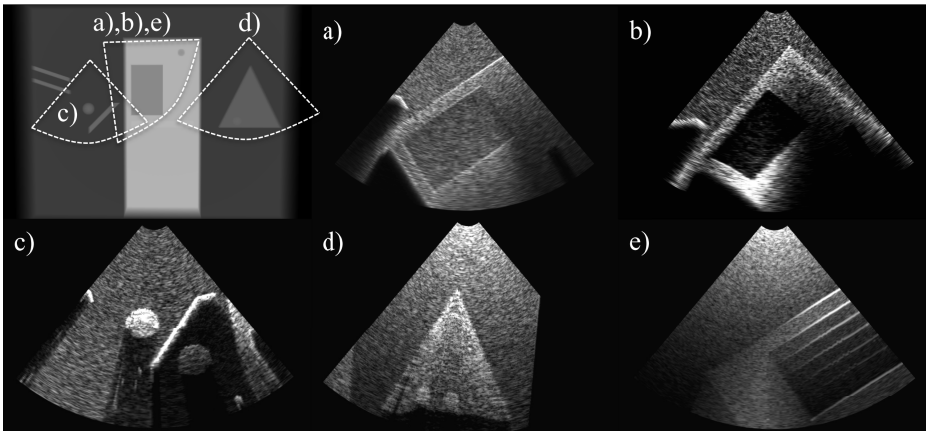

Fig. 2. Ultrasound artifacts exhibited in the artificial phantom (top left). a) Shadowing, b) Range distortion due to (exaggerated) speed of sound differences in tissue, c) mirroring, d) refraction and e) reverberation

3.3 Quantitative Evaluation and Optimization

For the evaluation of the statistical characteristics, the simulation was performed on a random scatterer volume with pixel dimension of 20 μm^3 and density of 1250 per mm^3 [11]. When using an unfocused beam-profile, intensity distribution for the produced analytic signal is known to follow Rayleigh statistics [12]. The result for the distribution fit is shown in Fig. 4. The sum of squares due to errors (SSE) was $3.14e$-05, which can be considered simlarly low as in literature [5], even though a direct comparison would require exactly identical source data. The goodness-of-fit between the measured histogram and its Rayleigh fit demonstrates that our simulation can produce accurate speckle characteristics despite the complex decomposition of the 3D convolution between separate rays. Please note that only envelope-detected, reflection/refraction-free data was used in this experiment, without post-processing.

Performance: Simulation performance is dependent on scatterers size, image depth, axial resolution, and depth of the rays binary tree. Simulation time including post-processing lies between 0.1-1s, which mainly depends on the number of scan-lines, depth of reflections, and axial resolution of the RF data (OpenCL implementation run on a laptop with NVIDIA GTX 850M). We also limited the binary trees depth to six since further reflections usually do not contribute significantly to the final image due to reduced ray intensities.

Optimization: Table 1 shows the parameters after optimization on 14 datasets; the visual appearance significantly improved in all cases. An exemplary result is shown in Fig. 3. The values for μ_0 and μ_1 are more consistent, while σ_0 and α vary for different patients. An explanation is that the latter two depend on log-compression and TGC parameters which are being simultaneously optimized.

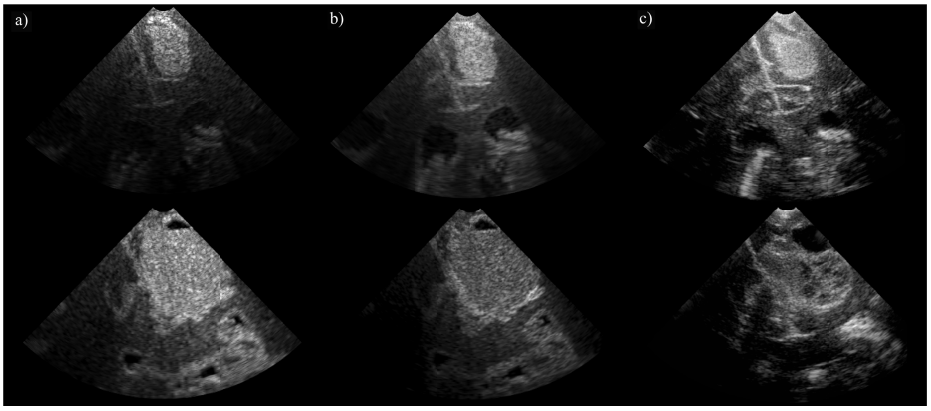

Fig. 3. Columns show (a): Simulation before optimization, (b): after optimization, (c): real US image. Both rows show a tumor next to the cerebral falx. Inaccuracies in b) are caused by segmentation errors (partly due to brain-shift) and the assumption of homogeneous scatterer properties per tissue type.

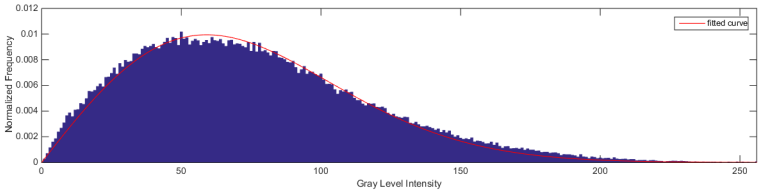

Fig. 4. Rayleigh Distribution Fit. $\sigma = 59.09$, SSE $= 3.14e$-05

Table 1. α, μ_0, σ_0, and μ_1 are brain white-matter's acoustic properties. μ and σ are mean and standard deviation of acoustic parameters after optimization.

AC	Initial	Optimized Parameters for each Patient														Statistics	
Prop.	Values	1	2	3	4	5	6	7	8	9	10	11	12	13	14	μ	σ
α	0.54	0.59	0.71	0.43	0.59	0.28	0.31	0.57	0.93	0.20	0.44	0.24	0.25	0.39	0.34	0.452	0.207
μ_0	0.40	0.40	0.36	0.06	0.37	0.33	0.39	0.44	0.40	0.30	0.30	0.32	0.34	0.27	0.32	0.332	0.089
σ_0	0.15	0.16	0.05	0.31	0.38	0.07	0.07	0.26	0.24	0.01	0.07	0.01	0.23	0.13	0.23	0.163	0.119
μ_1	0.00	0.00	0.00	0.04	0.00	0.00	0.00	0.00	0.01	0.00	0.00	0.00	0.00	0.00	0.00	0.004	0.013

4 Conclusion

We have presented a patient-specific US simulation from MRI at interactive frame rates, using a hybrid, convolutional ray-tracing approach with limited data pre-processing. Furthermore, for the first time, we propose a similarity formulation for optimization of both US system and tissue acoustic parameters. This improves simulation realism and further closes the gap between underlying physics and information contents of both modalities. Possible applications go

beyond typical usages of ultrasound simulation today. For example, pre-operative tissue appearance anticipation from MRI and planning of transducer positioning could help with tight time constraints in US-guided interventions. A shortcoming of our simulation is its high dependence on the segmentation accuracy. Future work could address this with a hybrid model for the scatterers texture, which combines the label map with original intensities of MRI/CT source data. The simulation and optimization accuracy should be also further evaluated, ideally in a controlled acquisition environment with known tissue parameters.

Acknowledgments. Bayerische Forschungsstiftung (BFS) grant RoBildOR and Deutsche Forschungsgesellschaft (DFG) grant BO 1895/4-1.

References

1. Bamber, J.C., Dickinson, R.J.: Ultrasonic B-scanning: a computer simulation. Physics in Medicine and Biology 25(3), 463–479 (1980)
2. Bürger, B., Bettinghausen, S., Rädle, M., Hesser, J.: Real-time GPU-based ultrasound simulation using deformable mesh models. IEEE Transactions on Medical Imaging 32(3), 609–618 (2013)
3. Comaniciu, D., Ramesh, V., Meer, P.: Kernel-based object tracking. IEEE Transactions on Pattern Analysis and Machine Intelligence 25, 564–577 (2003)
4. Gao, H., Choi, H.F., Claus, P., Boonen, S., Jaecques, S., Van Lenthe, G.H., Van der Perre, G., Lauriks, W., D'hooge, J.: A fast convolution-based methodology to simulate 2-D/3-D cardiac ultrasound images. IEEE Transactions on Ultrasonics, Ferroelectrics, and Frequency Control 56(2), 404–409 (2009)
5. Gao, H., Hergum, T.T.R., Torp, H., D'hooge, J.: Comparison of the performance of different tools for fast simulation of ultrasound data. Ultrasonics 52(5), 573–577 (2012)
6. He, K., Sun, J., Tang, X.: Guided image filtering. In: Daniilidis, K., Maragos, P., Paragios, N. (eds.) ECCV 2010, Part I. LNCS, vol. 6311, pp. 1–14. Springer, Heidelberg (2010)
7. Hedrick, W.R., Starchman, D.E., Hykes, D.L.: Ultrasound physics and instrumentation, 4th edn. Elsevier Mosby, St. Louis (2005)
8. Jensen, J.A.: A multi-threaded version of Field II. In: 2014 IEEE International Ultrasonics Symposium, pp. 2229–2232, September 2014
9. Karamalis, A., Wein, W., Navab, N.: Fast ultrasound image simulation using the Westervelt equation. In: Jiang, T., Navab, N., Pluim, J.P.W., Viergever, M.A. (eds.) MICCAI 2010, Part I. LNCS, vol. 6361, pp. 243–250. Springer, Heidelberg (2010)
10. Mercier, L., Del Maestro, R., Petrecca, K., Araujo, D., Haegelen, C., Collins, D.: Online Database of Clinical MR and Ultrasound Images of Brain Tumors. Medical Physics 39, 3253 (2012)
11. Meunier, J., Bertrand, M.: Ultrasonic texture motion analysis: theory and simulation. IEEE Transactions on Medical Imaging 14(2), 293–300 (1995)

12. Wagner, R.F., Insana, M.F., Brown, D.G.: Statistical properties of radio-frequency and envelope-detected signals with applications to medical ultrasound. Journal of the Optical Society of America. A, Optics and image Science 4, 910–922 (1987)
13. Wein, W., Brunke, S., Khamene, A., Callstrom, M., Navab, N.: Automatic CT-Ultrasound Registration for Diagnostic Imaging and Image-Guided Intervention. Medical Image Analysis 12(5), 577 (2008)
14. Zhang, Y., Brady, M., Smith, S.: Segmentation of brain mr images through a hidden markov random field model and the expectation-maximization algorithm. IEEE Transactions on Medical Imaging 20(1), 45–57 (2001)